

Landslides (2011) 8:417–432
 DOI 10.1007/s10346-011-0258-8
 Received: 18 August 2010
 Accepted: 11 February 2011
 Published online: 2 April 2011
 © Springer-Verlag 2011

Behzad Ataie-Ashtiani · Saeedeh Yavari-Ramshe

Numerical simulation of wave generated by landslide incidents in dam reservoirs

Abstract In this work, a two-dimensional fourth-order Boussinesq-type numerical model is applied to estimate the impact of landslide-generated waves in dam reservoirs. This numerical model has recently been extended for simulating subaerial landslides. The extended model is validated using available three-dimensional experimental data, and a good agreement is obtained. The numerical model is then employed to investigate the impact of landslide-generated waves in two real cases, the Maku and Shafa-Roud dam reservoirs in the northwestern and the north of Iran, respectively. Generated wave heights, wave run-up, maximum wave height above dam crest, and dam overtopping volume have been estimated for each case. The amplitude of generated waves about 18 and 31 m and the volume of dam overtopping up to 80,000 m³ emphasize the importance of the estimation of the landslide-generated waves in dam sites.

Keywords Impulsive waves · Submarine/subaerial landslide · Overtopping · Run-up · Boussinesq-type model · Case study

Introduction

Estimation of landslide-generated wave's characteristics is of the utmost importance in the dam engineering and water reservoir planning. Any type of geophysical mass flow, in dam reservoirs, such as debris flows, debris avalanches, landslides, and rock falls may generate horrible impulsive waves that can cause serious damages to reservoir sidewalls, dam body, adjacent hydraulic structures, and agricultural or residential areas (Semenza 2000). Moreover, a huge sliding mass decreases the efficient capacity of dam reservoirs and initiates subsequent economical damages. For example, one of the most catastrophic rockslide-generated-impulsive waves in the world happened in the Vaiont reservoir in 1963, overtopping the arch dam by more than 100 m. The village of Longarone, located in the downstream of the dam, was completely destroyed with almost 3,000 fatalities (Panizzo et al. 2005). Therefore, it is very important to estimate the characteristics of landslide-generated waves in dam reservoirs.

Four distinct stages can be distinguished in simulating landslide-generated waves in dam reservoirs: the generation, the propagation, the overtopping, and the run-up stages (Fig. 1). In the present study, each of these stages is considered in simulating landslide-induced wave scenarios for the Maku and the Shafa-Roud dam reservoirs.

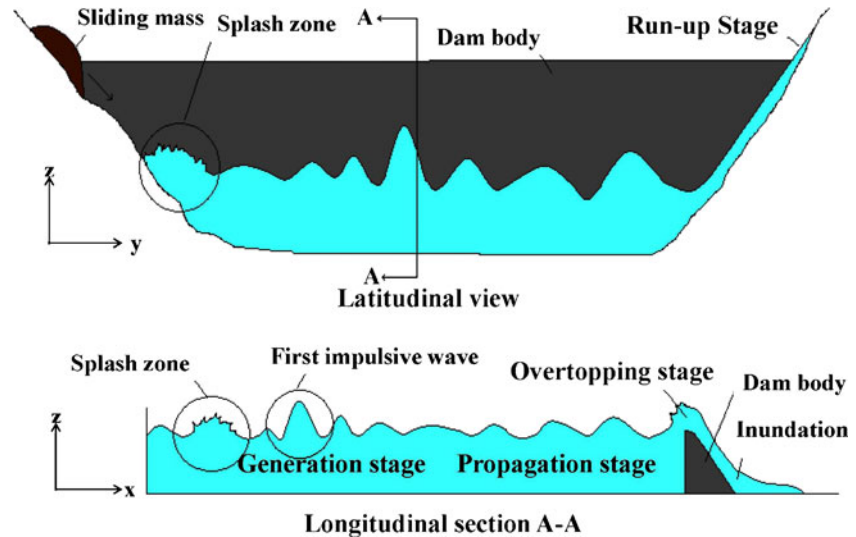
A large number of experimental and numerical studies have been conducted concerning the landslide-generated waves. A comprehensive review of these studies can be found in (Ataie-Ashtiani and Najafi-Jilani 2006). Most of the experimental studies are concerned about investigating effective parameters and characteristics of subaerial (Ataie-Ashtiani

and Nik-khah 2008; Carvalho and Carmo 2007; Risio et al. 2009; Shigihara et al. 2006; Zweifel et al. 2006) and submarine (Enet and Grilli 2005; Grilli and Watts 2005; Liu et al. 2005; Najafi-Jilani and Ataie-Ashtiani 2007) landslide-generated waves. In numerical studies, the developed models can be categorized according to their mathematical formulations as the Boussinesq-type models (Ataie-Ashtiani and Najafi-Jilani 2007; Hanes and Inman 1985; Lynett and Liu 2002), models developed based on non-linear shallow water (NSW) wave equations (Fernandez-Nieto et al. 2008; Medina et al. 2008; Saut 2003) and potential flow equations (Grilli et al. 2002; Grilli and Watts 2005). Furthermore, some researchers have utilized the developed numerical models for simulating landslide-generated waves in real cases (Ataie-Ashtiani and Malek-Mohammadi 2007; Heidarzadeh et al. 2008; Heinrich et al. 2001; Mader 2002; Pastor et al. 2008). For example, Ataie-Ashtiani and Malek-Mohammadi (2007) proposed two new empirical equations for estimating the near-field wave amplitude and velocity of subaerial-landslide-generated waves based on the observed data of real cases (Ataie-Ashtiani and Malek-Mohammadi 2007). Then they used estimated first wave characteristics as input data of the FUNWAVE numerical model (Kirby et al. 1998) for simulating three landslide scenarios of the Shafa-Roud dam reservoir (Ataie-Ashtiani and Malek-Mohammadi 2008).

In the present study, a two-dimensional fourth-order Boussinesq-type model developed by Ataie-Ashtiani and Najafi-Jilani (2007), entitled LS3D, is used for simulating landslide-generated waves of two real cases. In numerical modeling, the main concern in various approaches is the accuracy of approximate equations to describe the nonlinearity effects and frequency dispersion of waves. Regarding this, the Boussinesq-type models are more efficient than models developed based on NSW waves or potential flow equations (Ataie-Ashtiani and Najafi-Jilani 2007). The LS3D model has fourth order accuracy in considering the nonlinearity effects and frequency dispersion of waves (Ataie-Ashtiani and Najafi-Jilani 2007). Furthermore, the present model is able to simulate the generation, the propagation, and the run-up stages.

The LS3D model was originally developed to study submarine-landslide-generated waves. The model has recently been extended to be able to apply to the simulation of subaerial-landslide-generated waves. In the present study, the ability of the extended model in simulating subaerial-landslide-generated waves is validated using the available three-dimensional experimental data of Ataie-Ashtiani and Nik-khah (2008). The extended model is then applied to the Maku and Shafa-Roud dam reservoirs in Iran. Generated wave height, wave run-up, maximum wave height above the dam crest, and dam overtopping volume are estimated for two and three landslide scenarios, respectively.

Fig. 1 Sketch illustrating separation of the generation, the propagation, the run-up, and the overtopping stages



Numerical model

Mathematical formulation

The LS3D model is a two-dimensional depth-integrated numerical model, developed by Ataie-Ashtiani and Najafi-Jilani (2007), for simulating submarine-landslide-generated waves. This model is developed using a fourth-order Boussinesq approximation for an arbitrary time variable bottom boundary. The model has high accuracy in considering the nonlinearity effects and frequency dispersion of waves particularly for waves generated in inter-

mediate and deeper water areas (Ataie-Ashtiani and Najafi-Jilani 2007).

In the LS3D model, the mathematical formulations are derived based on a higher-order perturbation analysis using the expanded form of velocity components (Ataie-Ashtiani and Najafi-Jilani 2007).

The higher-order continuity equation in depth-integrated form (Eq. 1); the first main equation in the numerical model that is solved by the other two horizontal momentum equations (Eq. 3) is (Ataie-Ashtiani and Najafi-Jilani 2007):

$$\begin{aligned} & \frac{1}{\varepsilon} h_t + \zeta_t + \nabla \cdot \{ (\varepsilon \zeta + h) \mathbf{u}_0 + \mu^2 [\frac{-1}{6} (\varepsilon^3 \zeta^3 + h^3) \mathbf{A} + \frac{1}{2} \tilde{z}^2 (\varepsilon \zeta + h) \mathbf{A} - \frac{1}{2} (\varepsilon^2 \zeta^2 - h^2) (\nabla \cdot \mathbf{B}) + \tilde{z}^2 (\varepsilon \zeta + h) (\nabla \cdot \mathbf{B})] \\ & + \mu^4 [\frac{1}{120} (\varepsilon^5 \zeta^5 + h^5) \nabla (\nabla \cdot \mathbf{A}) - \frac{1}{24} (\varepsilon \zeta + h) \tilde{z}^4 \nabla (\nabla \cdot \mathbf{A}) - \frac{1}{12} (\varepsilon^3 \zeta^3 + h^3) \nabla (\nabla \cdot (\tilde{z}^2 \cdot \mathbf{A})) \\ & + \frac{1}{4} (\varepsilon \zeta + h) \tilde{z}^2 \nabla (\nabla \cdot (\tilde{z}^2 \cdot \mathbf{A})) + \frac{1}{24} (\varepsilon^4 \zeta^4 - h^4) \nabla (\nabla \cdot (\nabla \mathbf{B})) - \frac{1}{6} (\varepsilon \zeta + h) \tilde{z}^3 \nabla (\nabla \cdot (\nabla \mathbf{B})) \\ & - \frac{1}{6} (\varepsilon^3 \zeta^3 + h^3) \nabla (\nabla \cdot (\tilde{z} \nabla \mathbf{B})) + \frac{1}{2} (\varepsilon \zeta + h) \tilde{z} \nabla (\nabla \cdot (\tilde{z} \nabla \mathbf{B})) \\ & + \frac{1}{2} (\varepsilon^2 \zeta^2 - h^2) \nabla C - (\varepsilon \zeta + h) \tilde{z} \nabla C \} = O(\varepsilon^6, \mu^6) \end{aligned} \quad (1)$$

where the nonlinearity ratio $\varepsilon = a_0/h_0$ and the frequency dispersion ratio $\mu = h_0/l_0$ show the nonlinearity effects and frequency dispersion of waves, respectively, in which a_0 is the impulsive wave amplitude, h_0 the characteristic water depth and l_0 the horizontal length scale. x and y are the horizontal coordinates scaled by l_0 , z is the vertical coordinate scaled by h_0 , t is time and scaled by $l_0/(gh_0)^{1/2}$, ζ is the water surface displacement scaled by a_0 , h is the total depth measured from the still water surface to the moving bottom boundary and scaled by h_0 , \mathbf{u} is the vector of horizontal velocity components (u , v) scaled by $\varepsilon(gh_0)^{1/2}$, w is the velocity in the vertical direction scaled by $(\varepsilon/\mu)(gh_0)^{1/2}$, p is the water pressure scaled by γa_0 , and $\nabla = (\partial/\partial x, \partial/\partial y)$ is the horizontal gradient vector. The subscripts

denote the partial derivative. The vector $\mathbf{A} = \nabla(\nabla \cdot \mathbf{u}_0)$, the parameter $B = \nabla \cdot (h \mathbf{u}_0) + \frac{1}{\varepsilon} h_t$, the parameter C (Ataie-Ashtiani and Najafi-Jilani 2007)

$$\begin{aligned} C = & \frac{1}{6} h^3 \nabla \cdot \mathbf{A} - \frac{1}{2} h \nabla \cdot (\tilde{z}^2 \cdot \mathbf{A}) + \frac{1}{2} h^2 \nabla \cdot (\nabla \mathbf{B}) - h \nabla \cdot (\tilde{z} (\nabla \mathbf{B})) \\ & + \frac{1}{2} h^2 \mathbf{A} \nabla h - \frac{1}{2} \tilde{z}^2 \mathbf{A} \nabla h - h \nabla h \nabla \mathbf{B} - \tilde{z} \nabla h \nabla \mathbf{B} \end{aligned} \quad (2)$$

and \tilde{z} is the characteristic depth chosen for the calculation of the horizontal velocity components, which is a weighted average of the two distinct water depths; z_a and z_b , described in the normalized form as $\tilde{z} = [\beta z_a + (1 - \beta) z_b]$, in which β is a weighting parameter which can be optimized in the verification stage (Gobbi et al. 2000).

The expanded forms of \mathbf{u} and w and the water pressure at $z = 0$ are substituted in the horizontal momentum equation to

create the other two main governing equations (Ataie-Ashtiani and Najafi-Jilani 2007):

$$\begin{aligned} \mathbf{u}_{0t} + \varepsilon(\nabla \cdot \mathbf{u}_0)\mathbf{u}_0 + \varepsilon(w_1|_{z=0})\mathbf{u}_{0z} + \mu^2[\mathbf{u}_{1t}|_{z=0} + \varepsilon(\nabla \cdot (\mathbf{u}_1|_{z=0}))\mathbf{u}_0 + \varepsilon(\nabla \cdot \mathbf{u}_0)(\mathbf{u}_1|_{z=0}) + \varepsilon(w_2|_{z=0})\mathbf{u}_{0z} + (w_1|_{z=0})(\mathbf{u}_{1z}|_{z=0})] \\ + \mu^4[\mathbf{u}_{2t}|_{z=0} + \varepsilon(\nabla \cdot (\mathbf{u}_2|_{z=0}))\mathbf{u}_0 + \varepsilon(\nabla \cdot (\mathbf{u}_1|_{z=0}))(\mathbf{u}_1|_{z=0}) + \varepsilon(\nabla \cdot \mathbf{u}_0)(\mathbf{u}_2|_{z=0}) + \varepsilon(w_2|_{z=0})(\mathbf{u}_{1z}|_{z=0}) + (w_1|_{z=0})(\mathbf{u}_{2z}|_{z=0})] \\ + \nabla(P|_{z=0}) = O(\varepsilon^6, \mu^6) \end{aligned} \quad (3)$$

In the perturbation analysis, the velocity domain components, \mathbf{u} and w , are expanded into $\mathbf{u} = \mathbf{u}_0 + \mu^2\mathbf{u}_1 + \mu^4\mathbf{u}_2$ and $w = \mu^2w_1 + \mu^4w_2$, respectively, where μ^2 is a basic small parameter in the analysis.

A sixth-order multi-step finite difference method is applied for spatial discretization and a sixth-order Runge-Kutta method is applied for temporal discretization of the higher-order depth-integrated governing equations and boundary conditions (Ataie-Ashtiani and Najafi-Jilani 2007). The model is validated using the available three-dimensional wave data obtained by the experimental submarine landslides.

Sliding mass simulation

In the present model, the sliding block geometry is defined using a truncated hyperbolic secant function. The landslide block motion is expressed as (Ataie-Ashtiani and Najafi-Jilani 2007):

$$S(t) = S_0 \ln \left(\cosh \frac{t}{t_0} \right) \quad (4)$$

where S is the location of the center of the sliding mass parallel to the sliding slope, $S_0 = u_t^2/a_s$ and $t_0 = u_t/a_s$, in which u_t and a_s are the terminal velocity and initial acceleration of the sliding block, respectively, and they are defined as (Ataie-Ashtiani and Najafi-Jilani 2007):

$$u_t = \sqrt{gB} \sqrt{\frac{\pi(\gamma - 1)}{2C_d}} \sin \theta, \quad a_s = g \frac{\gamma - 1}{\gamma + C_m} \sin \theta \quad (5)$$

where $\gamma = \rho_l/\rho_w$, B is the length of sliding block along the inclined bed, C_d is the drag coefficient, C_m is the added mass coefficient, θ is the bed slope and g is the acceleration due to gravity. ρ_l and ρ_w are the densities of landslide block and water, respectively. With the transformation of Eq. 4 from the bed slope direction to the principal x , y , and z directions, the equation of sliding mass movement is obtained. Accordingly, the geometry of the bed is described as a time-variable bottom boundary (Ataie-Ashtiani and Najafi-Jilani 2007). For example, in a simplified condition (one-dimensional condition), the equation of the sliding mass is given as

$$\begin{aligned} h(x, t) = h_0(x) - 0.5T \left[1 + \tanh \left(\frac{x - x_l(t)}{S} \right) \right] \\ \times \left[1 - \tanh \left(\frac{x - x_r(t)}{S} \right) \right] \end{aligned} \quad (6)$$

where $x_l(t) = x_c(t) - 0.5T \cos \theta$ and $x_r(t) = x_c(t) + 0.5T \cos \theta$ are the locations of the rear and the front ends of the sliding mass, respectively. $x_c(t)$ is the location of the sliding mass center, T is the maximum mass thickness, and $S = 0.5/\cos \theta$. Equation 6 describes the location of the sliding mass center at an arbitrary time (Ataie-Ashtiani and Najafi-Jilani 2007). A schematic of the parameters are shown in Fig. 2.

This approach is extended to the three-dimensional conditions by Enet et al. (2003). They use a truncated hyperbolic secant function of x and y with a specific truncation ratio, r , for describing the landslide model geometry, and verified that function by both the experimental and the real landslide case data (Enet et al. 2003).

$$\begin{aligned} z(x, y) = \frac{T}{r} [\text{sech}(K_w x) \cdot \text{sech}(K_b y) - (1 - r)]; \text{ for } z \geq 0 \\ K_w = \frac{2}{w} \text{asech} \left(\frac{1-r}{r} \right) \text{ and } K_b = \frac{2}{B} \text{asech} \left(\frac{1-r}{r} \right) \end{aligned} \quad (7)$$

where z is the thickness of sliding mass on the sliding bed. The specific truncation ratio can be modified according to real geometry of sliding mass. This extended approach is applied in the present numerical model (details can be found in (Ataie-Ashtiani and Najafi-Jilani 2007); (Gobbi et al. 2000)).

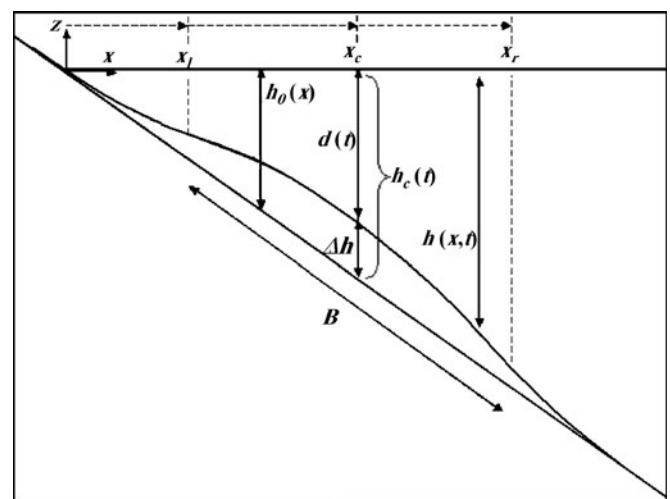


Fig. 2 Schematic of the sliding mass parameters

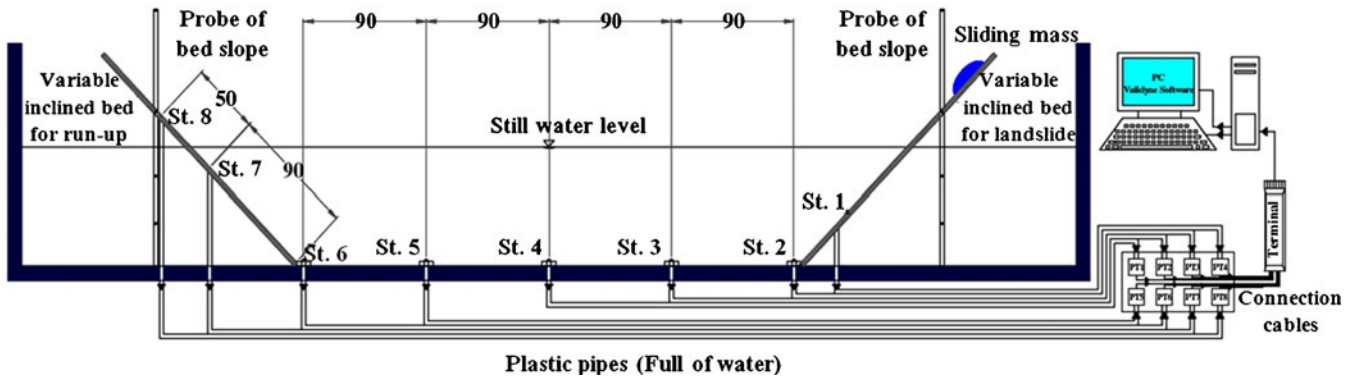


Fig. 3 Schematics of the experimental set up for subaerial-landslide-generated waves, all dimensions are in centimeter (Ataie-Ashtiani and Nik-khah 2008)

In the numerical model, the surface of the sliding mass is considered as a time-variable bottom boundary. The kinematic boundary condition of the bed is (Ataie-Ashtiani and Najafi-Jilani 2007; Gobbi et al. 2000):

$$h_t + \mathbf{u} \cdot \nabla h = -w \quad \text{on } z = -h \quad (8)$$

The details of the method to enter the bottom boundary condition into the system of numerical model equations can be found in (Ataie-Ashtiani and Najafi-Jilani 2007).

Numerical model extension

The LS3D model has recently been extended to study subaerial-landslide-generated waves based on the method of Lynett and Liu (2005). According to Eqs. 4 and 5, the kinematic characteristics of sliding mass depend on the terminal velocity of the solid block, u_t , and its initial acceleration, a_s . Lynnet and Liu proposed that when the sliding mass is initially subaerial, the equation of sliding mass velocity must be altered to include the aerial acceleration. Accordingly, they formulated the sliding velocity as a

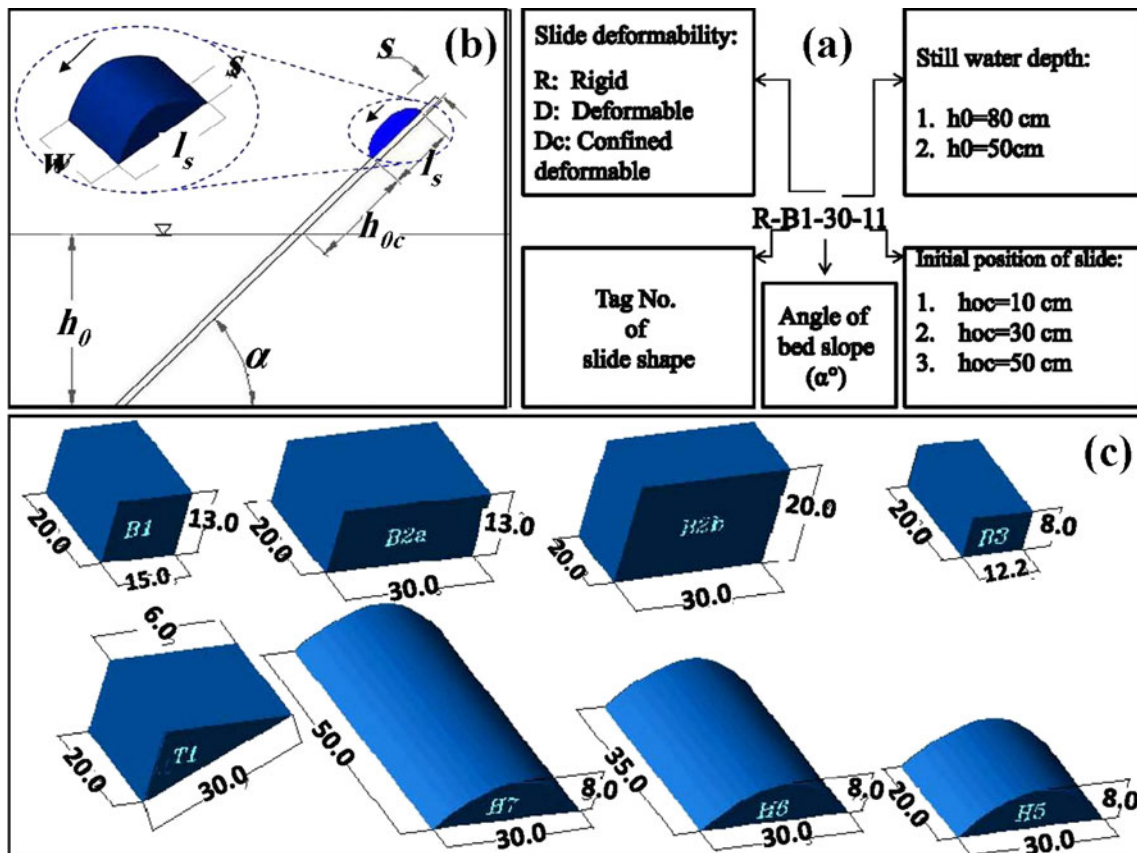
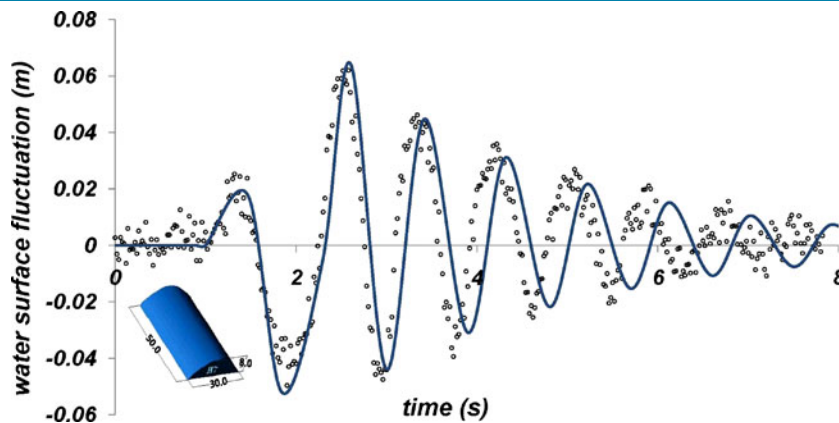


Fig. 4 a The test numbering procedure, b the schematic of the geometric parameters of each case: the slide slope, α , width, w , thickness, S , length parallel to the bed slope, l_s , and initial distance from water surface, h_{0c} and the still-water depth, h_0 , and c various geometries and dimensions of each test (Ataie-Ashtiani and Nik-khah 2008)

Fig. 5 Comparison of the numerical (solid line) and the experimental (open circles) results for subaerial-landslide-generated waves in the generation stage. Test R-H7-30-31 at ST 1



weighted average of the aerial and submerged velocities, where the weighting parameter is based on the fraction of the submerged volume (Lynett and Liu 2005). Thus, the slope-parallel velocity of the slide is given by

$$f_s u_s + f_a g t \sin \theta \quad (9)$$

The coefficients f_s and f_a represent the submerged and the aerial volume fractions of the landslide, respectively (between 0 and 1). The time-dependent velocity of a submerged landslide, u_s , is calculated as in (Grilli et al. 2002):

$$u_s = u_t \tanh\left(\frac{t}{t_0}\right) \quad (10)$$

This linear combination of the aerial and submerged velocities is used instead of terminal velocity, u_t , in Eq. 5. Although this approach is an approximate and simplified method of subaerial landslide modeling, the following comparison of the numerical and the experimental (Ataie-Ashtiani and

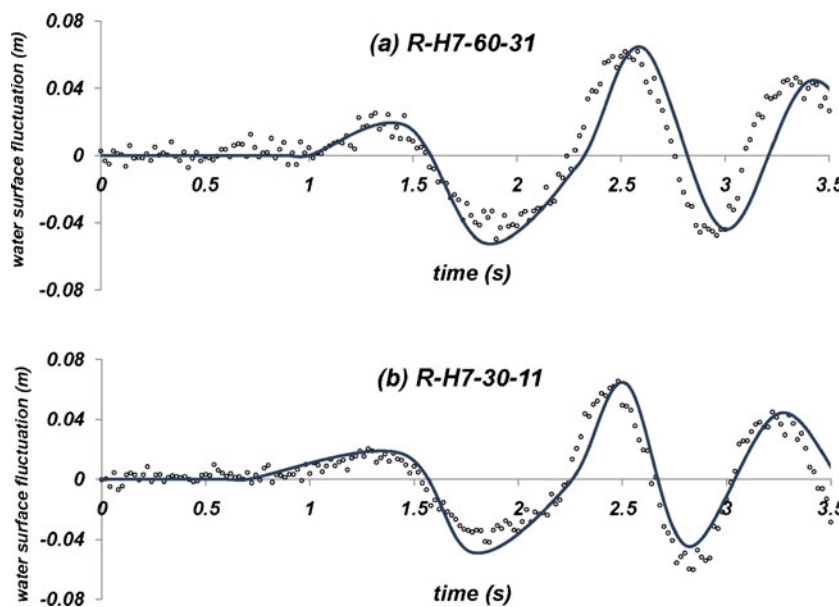
Nik-khah 2008) results shows that this method is really a good simplification for simulating subaerial-landslide-generated waves.

Numerical model application

Experimental data

Ataie-Ashtiani and Nik-khah (2008) performed 120 laboratory tests concerning with the subaerial-landslide-generated waves. The experiments were carried out in a 2.5-m wide, 1.8-m deep, and 25-m long wave tank. Two inclined steel planes with slopes adjustable from 15° to 60° were installed; one plane for sliding down the blocks, the other for observation of the run-up of landslide-generated waves. The sliding surface was smooth and also lubricated in order to provide a frictionless slope. The experimental sliding mass are either rigid, made of 2-mm thick steel sheet with various dimensions and shapes (wedge, cubic, and hyperbolic geometry, shown in Fig. 4c) or deformable, made of unconfined lump of sand, which initially has wedge shape or

Fig. 6 Differences between the experimental (open circles) and the numerical (solid line) results in the generated wave shapes depending on the different bed slopes and the slide initiation levels



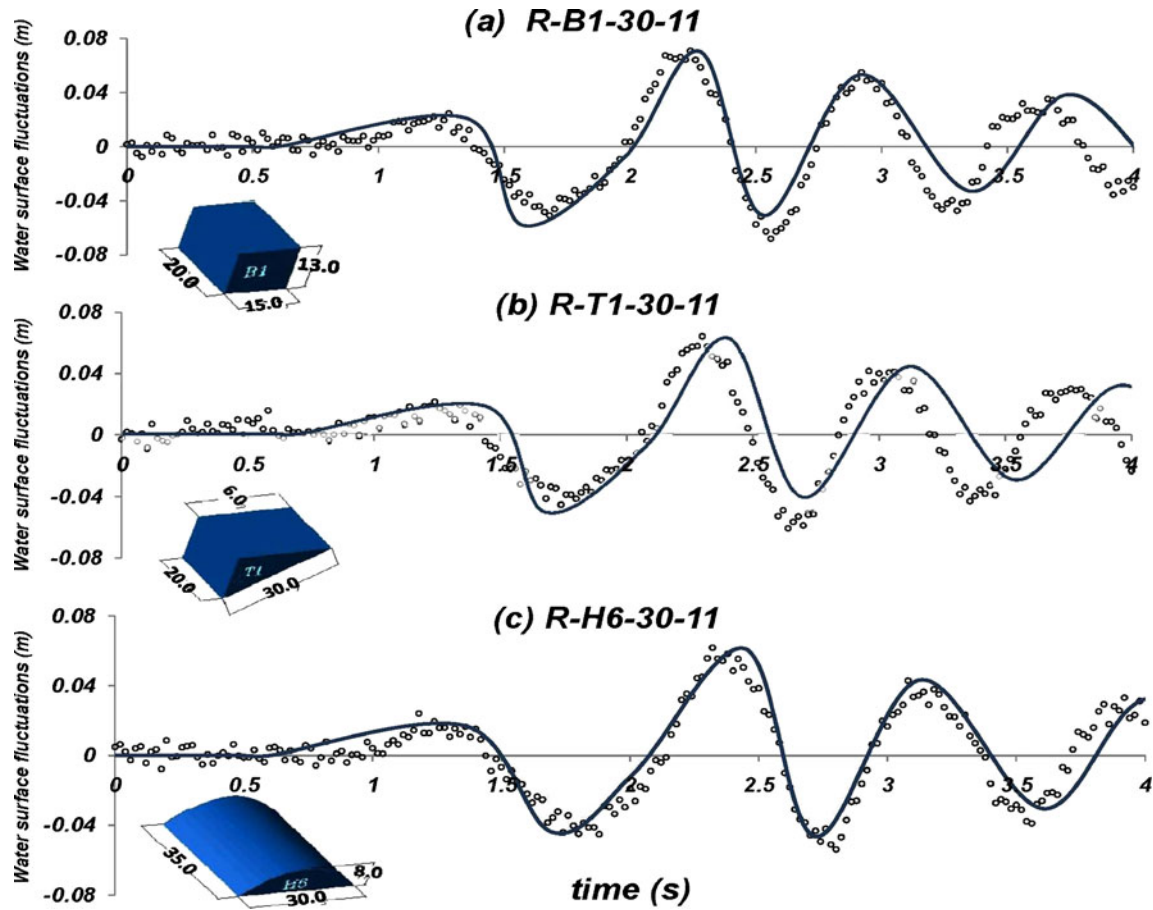


Fig. 7 Comparison between the numerical (solid line) and the experimental (open circles) results for various sliding mass geometries

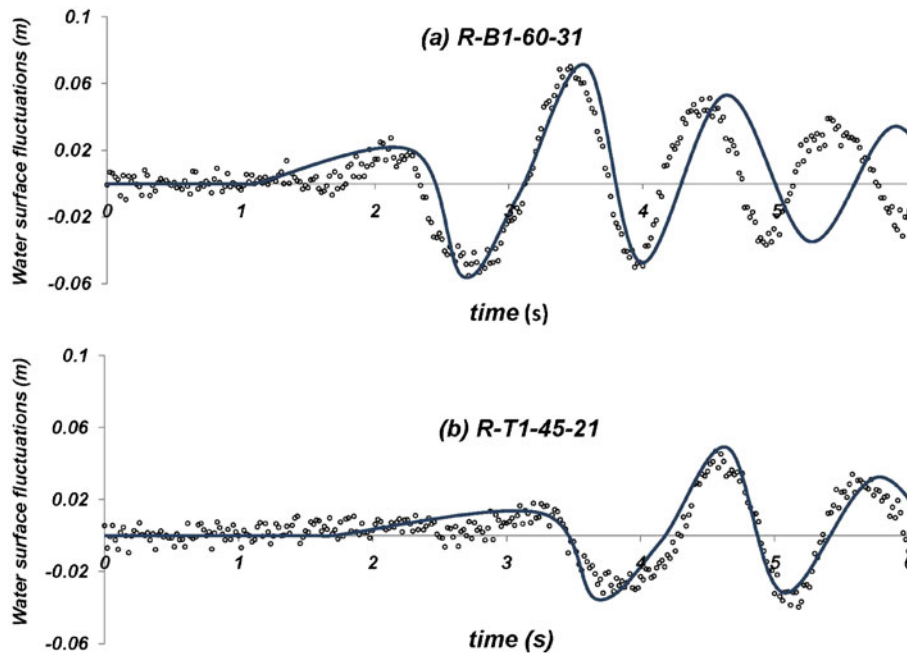


Fig. 8 Comparison between the numerical (solid line) and the experimental (open circles) results in the propagation stage at a fourth and b sixth gauge locations



Fig. 9 Location of the Maku dam, 11°39'17" N and 44°28'55" E. (Google earth map)

confined sand in a softly deformable lace. A schematic of the wave tank and the adjustable slopes is shown in Fig. 3. The Validyne DP15 differential pressure transducers were used as wave

gauges in the experiments. They were located at eight points along the central axis of the tank (ST1 to ST8 shown on Fig. 3) (Ataie-Ashiani and Nik-khah 2008). Further information on the experi-

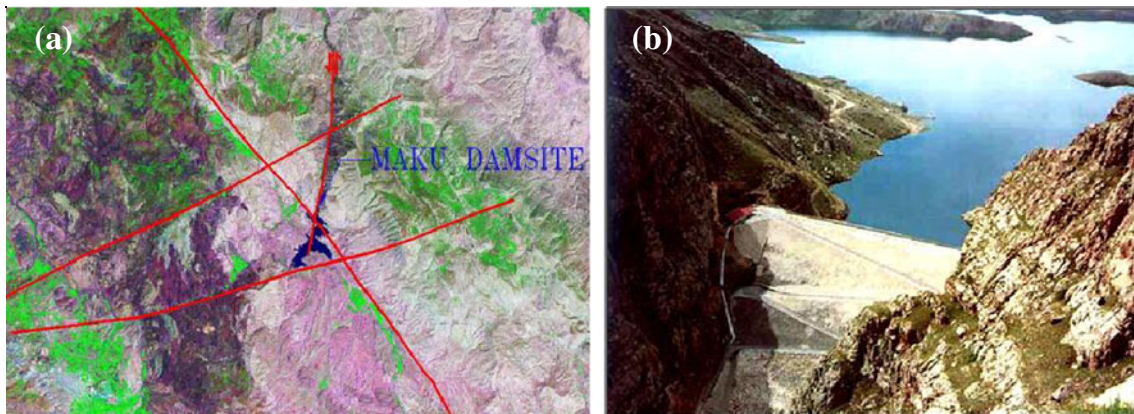


Fig. 10 a Satellite image of the Maku dam site and the existing faults (Mahab Ghods 1999a). b An oblique view of the Maku dam (Niro ministry 1999)

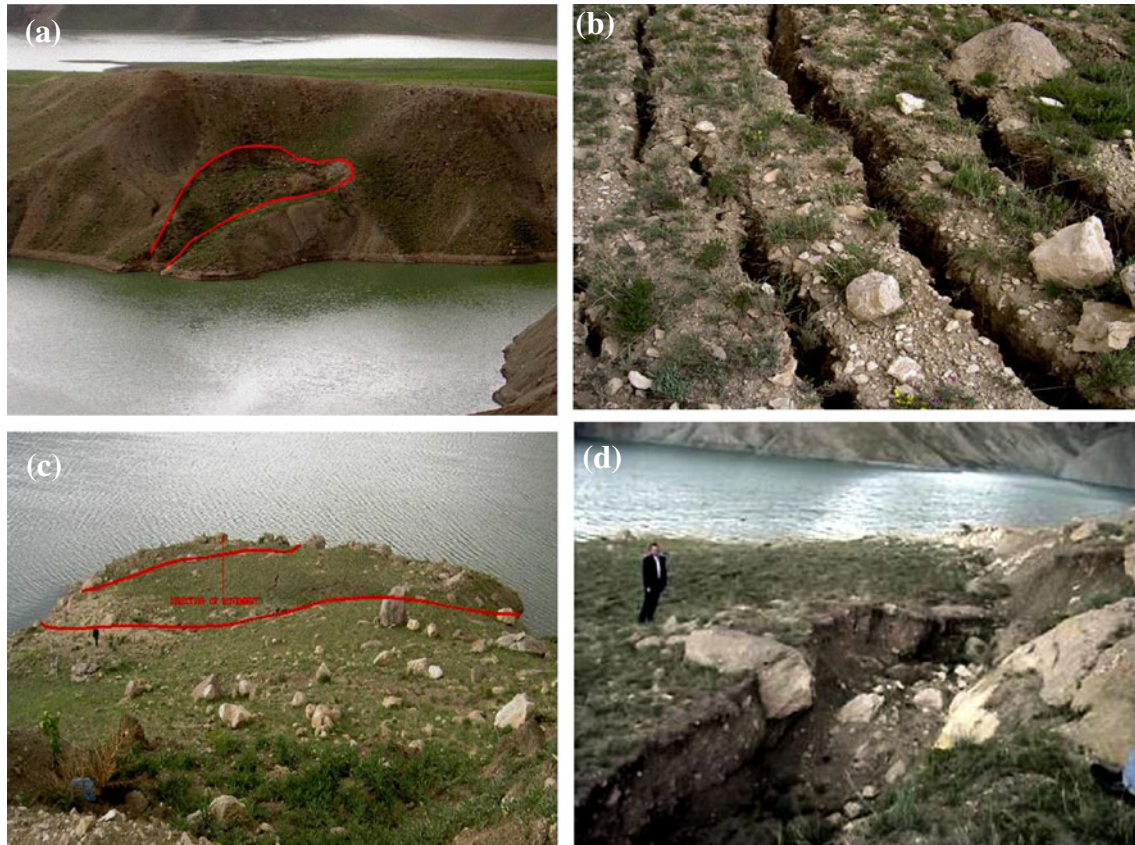


Fig. 11 a A possible slide on the east bank of the Maku dam reservoir, and b its zoom-view. c A possible slide on the west bank of the Maku dam reservoir, and d its zoom-view (Mahab Ghods 1999a)

ments can be found in (Ataie-Ashtiani and Nik-khah 2008; Najafi-Jilani and Ataie-Ashtiani 2007).

The specifications of each experiment can be observed by the test numbering scheme (Fig. 4a) (Ataie-Ashtiani and Nik-khah 2008). A schematic of the main parameters of the experiments is also shown in this figure. In the experiments, the spatial and temporal changes of the impulsive wave features, such as amplitude and period, are studied. Furthermore, the effects of bed slope angle, water depth, slide impact velocity and geometry of the mass on the shape, and deformation of landslide-generated waves are investigated (Ataie-Ashtiani and Nik-khah 2008; Najafi-Jilani and Ataie-Ashtiani 2007).

Numerical simulation

To make the calculation stable, the optimal values of time step, Δt , and grid dimensions in x and y directions, Δx and Δy , are chosen

based on the Courant number (Grilli and Watts 1999). Accordingly, the time step of 0.01 s and the grid dimensions of 0.1 m are selected.

Comparisons of numerical and experimental results

Comparisons between the experimental and the numerical results are performed concerning with the temporal water surface fluctuations recorded at the positions of gauges (ST1–ST8) shown in Fig. 3. The gauge locations and time intervals of the numerical model are exactly the same as the experimental set up.

Periods and amplitudes in generating stage

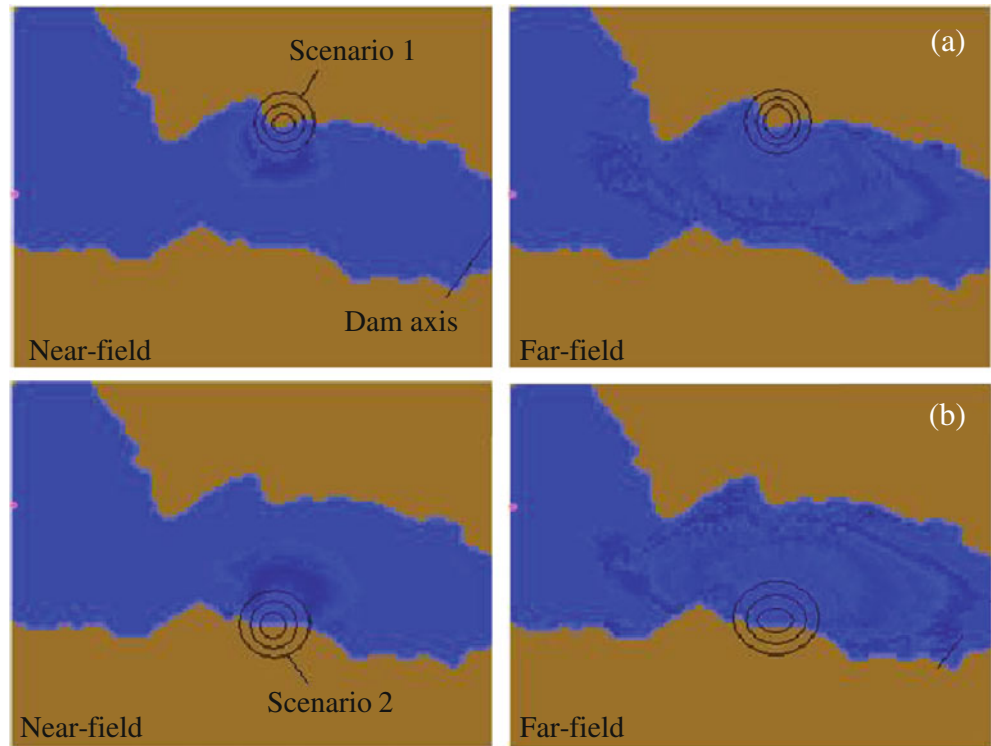
The time series of wave amplitude at ST1 gauge location (Fig. 3) for the R-H7-30-31 test is selected as a standard for the comparison of the numerical and the experimental results in the generation stage (Fig. 5), because its hyperbolic geometry of the sliding mass is the most appropriate

Table 1 Properties of two landslide scenarios of the Maku dam site

Scenario no.	B (m)	T (m)	γ	d (m)	α (deg)	V (mm^3)
1	80	15	1.9	-15	30	0.6
2	60	10	1.9	5	32	0.15

B slide length; T maximum slide thickness; γ relative slide density; d initial vertical distance of sliding mass from water surface; α slide slope; V slide volume

Fig. 12 (Top) Near and far fields generated wave expanses due to a west bank landslide; *Scenario 1*. (Bottom) Near and far fields generated wave expanses due to an east bank landslide; *Scenario 2*

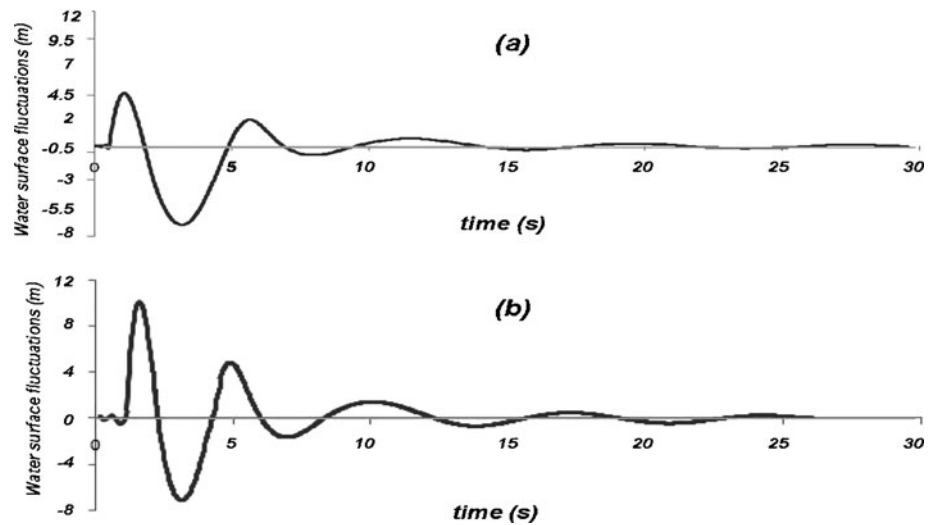


simplification of the real landslide geometries (Grilli et al. 2002; Lynett and Liu 2004) and the sliding masses are supposed to be rigid in the numerical model. In this comparison, the numerical and experimental results are in rather good agreement. A time phase difference of 10–15%, which makes the numerical wave steeper than the experimental wave, is observed. It may be due to the numerical dispersion that gradually makes the numerical results far from the experimental values. Furthermore, the two-dimensional simulation for the actual three-dimensional conditions

could be another reason, even though higher-order approximations are used to simulate fluid behavior in the vertical direction.

The first part of the time series in the case R-H7-60-31 is shown in Fig. 6a. According to this figure, the maximum positive and negative amplitudes of the numerical waves are 3.5% and 4.8% greater than those values in the experimental waves, respectively. For all the simulated tests, including the deformable sliding mass cases, the estimation error of wave amplitude is less than 5%, and for the majority cases, it is less

Fig. 13 Generated waves in the near field for a *Scenario 1* and b *Scenario 2*



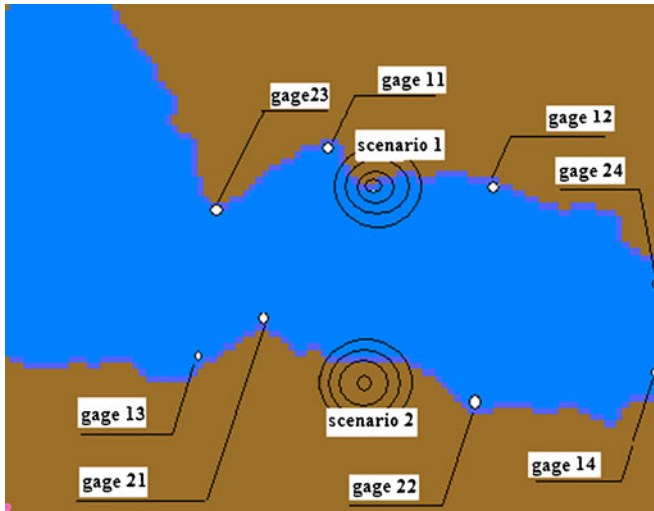


Fig. 14 Gauge locations for determining the wave run-up near the sidewalls and the Maku dam body (the first number of each gauge name is the number of scenario and the second one is the number of gauge)

than 1%. The period of waves generated by the deformable sliding masses, however, become larger than that due to a rigid mass, and it cannot be estimated by the present model because the model considers the mass not deformable.

Effects of the bed slope and the falling height

For the R-H7-60-31 test (Fig. 6a) the falling height and the bed slope are 0.433 m and 60°, respectively. Although in the case R-H7-30-11 (Fig. 6b), the sliding mass has the same shape as R-H7-60-31, the falling height and the bed slope are 0.05 m and 30°, respectively. When the subaerial falling height and bed slope are small, the amplitude of the second negative wave becomes greater than the amplitude of the first negative wave (see the experimental data in Fig. 6b). This is not the case of greater falling height and steeper bed slope (Fig. 5 and 6a). The numerical results, however, show that the first negative wave is always greater than the second negative wave, and this tendency seems to fit to the case of greater plunging velocity.

Table 2 Wave run-up at the Maku reservoir sidewalls

Gauge no.	X_p (m)	h_o (m)	β (deg)	a_c (m)	a_t (m)	H (m)	R (m)
11	70	50	23	2.19	5.71	7.9	22.2
12	90	50	35	1.35	4.07	5.42	10.5
13	168	50	48	1.75	4.23	5.98	9.5
14	280	50	25	2.42	4.56	6.98	17
21	90	50	20	4.7	5.22	9.9	30.7
22	100	50	70	3.8	2.6	6.38	6.5
23	135	50	65	4.25	2.5	6.74	7.8
24	245	50	25	5.62	2.9	8.5	22

X_p , distance from slide source; h_o , average depth of water; a_c , positive wave amplitude; a_t , negative wave amplitude

This discrepancy is likely due to the assumption in the LS3D model application for the simulation of subaerial-landslide-generated waves. As explained in Section 2.3, a linear combination of the slide plunging velocity and the underwater terminal velocity of the sliding mass is used as the kinematic condition of the slide. Thus, the generation mechanism of waves by a subaerial landslide is considered to be the same as the mechanism due to submarine landslide. In the submarine wave generation, the first negative wave has always the greatest amplitude and it diminishes subsequently. Hence, the present numerical model is not able to simulate greater second negative wave induced by a subaerial landslide having relatively small plunging velocity.

In any case, the main purposes of the landslide-generated wave simulation are to predict the maximum positive wave amplitude, wave run-up, and dam overtopping. As far as the positive wave amplitudes are concerned, no such discrepancies between the numerical results and the experiments are conspicuous as shown in Fig. 6a, b. Therefore, it can be said that the model is applicable for the purposes to estimate the hazards brought by the subaerial-landslide-generated waves.

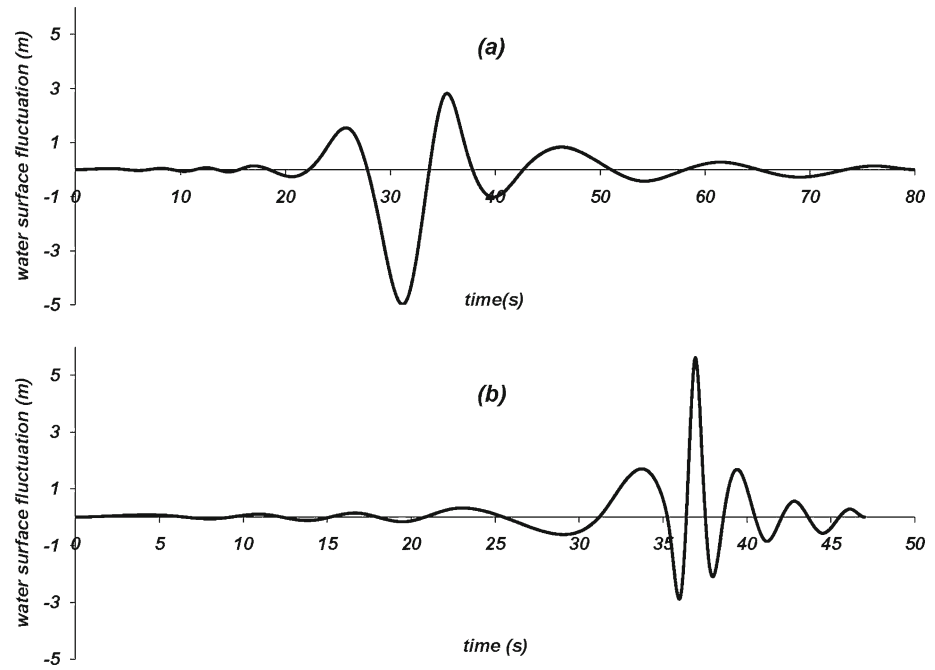
Effects of the sliding mass shape

To quantify differences between the numerical and the experimental results, the computational error in the first period of wave is computed by:

$$Err = \frac{\sum_{i=1}^n \left| \frac{\zeta_{Experimental} - \zeta_{Numerical}}{\zeta_{Experimental}} \right|}{n + 1} \quad (11)$$

where ζ is the water surface level, T_s is the first period of the generated wave and $n = \frac{T_s}{\Delta t}$. The numerical and experimental results in the wave generation stage for different sliding mass shapes are compared in Fig. 7. The results are in good agreement and the maximum computational error is approximately 3%. The sliding mass with hyperbolic geometry (H6) has a minimum computational error of 1.6% (Fig. 7c). In the LS3D model, the sliding block geometry is defined by a truncated hyperbolic secant function (see Section 2.2). Therefore, the sliding masses with hyperbolic geometries (H5, H6, and H7 with various dimensions) have better agreement with the experimental results than other geometries.

Fig. 15 Temporal water surface fluctuations nearby the Maku dam caused by a *Scenario 1* and b *Scenario 2*



Propagation stage

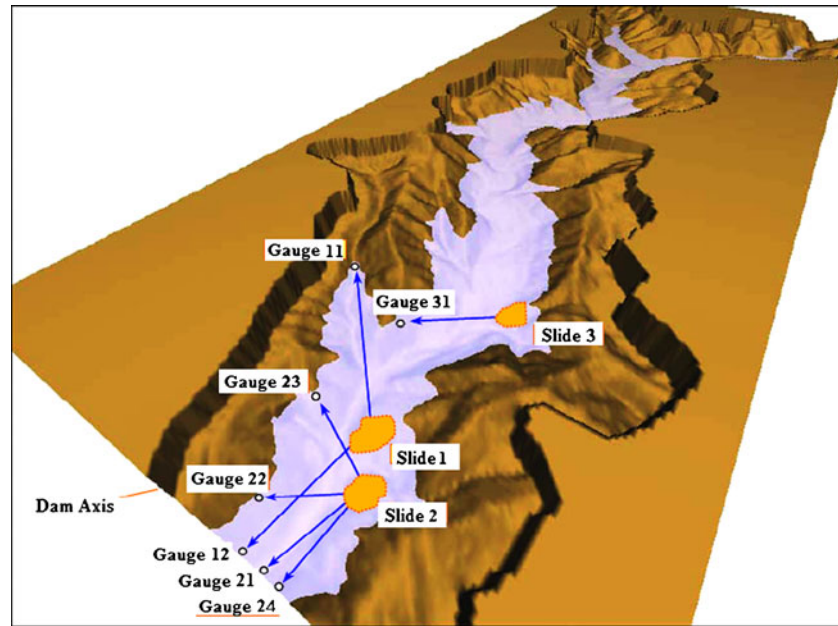
By comparing the numerical and the experimental results in the propagation stage, the ability of numerical simulations for wave

dispersion will properly be assessed. Consequently, the effects of higher order nonlinear components in Boussinesq-type equations may also be evaluated. In Fig. 8, the numerical and the experimental

Fig. 16 Location of the Shafa-Roud dam (37° 32' N and 49° 08' E) (Mahab Ghods 1999b)



Fig. 17 Location of the three slide areas considered and the gauge locations for estimating run-up height, the Shafa-Roud dam



data for two tests at the fourth and sixth gauge locations are shown. The estimation error of wave amplitude in the propagation stage is within 5%, and this is the same order as in the generation stage.

Case studies

Maku dam reservoir

Setting

The Maku dam is located in the southern part of the Maku town, West Azarbaijan province, Iran, on the Zangmar River. The Zangmar River originates in the mountains above the Maku town, along the Turkish–Iranian border, not far from Mount Ararat and flows south and east into the Araxes River at the town of Pol Dasht (Fig. 9). The dam is located in a seismic region (Fig. 10a). The Badavli fault is located near the dam site; thus, seismic conditions intensify its crucial landslide-susceptibility status (Mahab Ghods 1999a).

The Maku dam is a 75-m high earth dam with a reservoir capacity of 135 mm³ (Fig. 10b). The length and width of the dam are 350 and 10 m, respectively. The dam crest level is 1,690 m from the sea level (Mahab Ghods 1999a).

According to geological investigations (Mahab Ghods 1999a), multiple factors such as rainfall, successive freezing–melting, pore water pressure changes, sequential changes in

underground water level and weathering initiate the formation and extension of large number of tensile cracks along the Maku reservoir beaches (Fig. 11b), which form some areas of instability. One of the most dangerous areas of instability is located on the West beach with the horizontal distance of 235 m from the dam axis (Fig. 11c, d). Another significant area of instability is a circular shape instability located on the Eastern beach with the horizontal distance of 230 m from the dam axis (Fig. 11a).

According to the topographic map of the Maku dam site, the first landslide scenario on the West beach is submarine and the second scenario on the East beach is subaerial. This means that the center of gravity is under the water surface for the first scenario and above the water surface for the second one. In any case, landslide blocks in both scenarios are partly submerged and proper cases for simulation by the extended numerical model. The properties of each scenario, estimated from the topographic map and the geological reports (Mahab Ghods 1999a), are shown in Table 1.

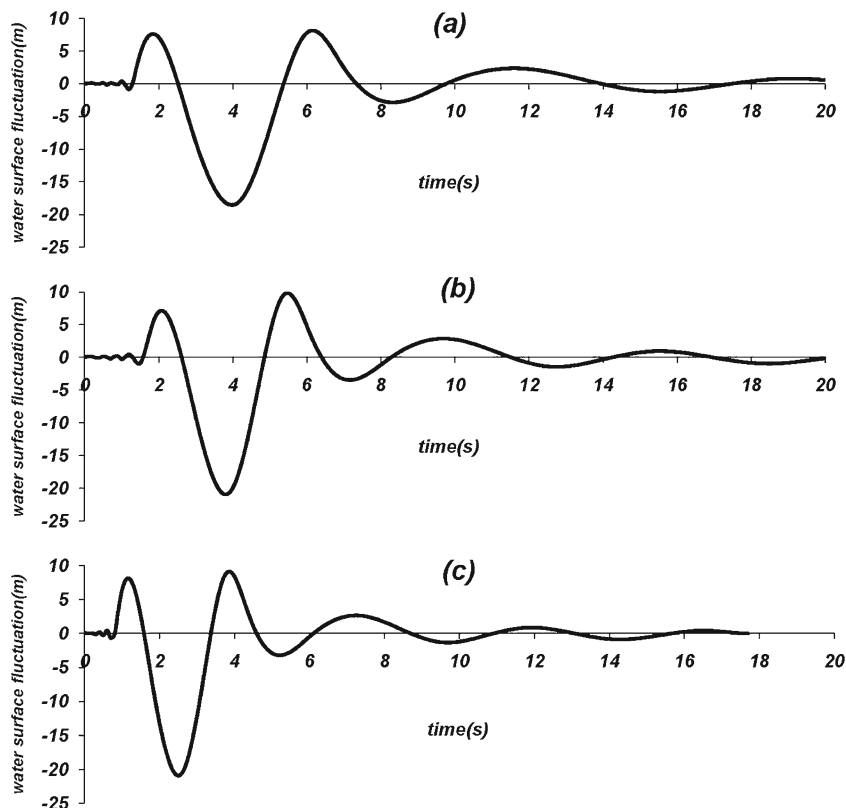
Simulation set up

Time step of 0.05 s, grid dimensions of 5×5 m in *x* and *y* directions, the three-dimensional topographic map (AutoCAD file) and the normal water level of 1,680 m are given to the program as input data. The grid mesh identifies the reservoir's

Table 3 The properties of the considered landslide scenarios, Shafa-Roud dam (definition of the parameters are in Table 1)

Scenario no.	<i>B</i> (m)	<i>T</i> (m)	γ	<i>d</i> (m)	α (deg)	<i>V</i> (mm ³)
1	380	15	2.7	−35	30	1
2	235	25	2.7	−30	30	1.4
3	140	30	2.7	−20	25	1

Fig. 18 Generated waves in the near field due to a Slide 1 (*Scenario 1*), (b) Slide 2 (*Scenario 2*), and (c) Slide 3 (*Scenario 3*), the Shafa-Roud dam site



shore in the case of normal water level as well as the computational borders.

The effects of reservoir side banks on waves, i.e., the effects of drying/wetting succession at the borders, is considered by introducing a reflection factor (Ataie-Ashtiani and Najafi-Jilani 2007). This factor shows that what percent of reaching waves to the computational domain borders return to the water body and what percent is damped. This factor, which depends on material and vegetation types of the reservoir sides, is estimated approximately as 0.6.

Results

According to the corrected mesh, generated by the LS3D model, the average length and width of the Maku dam reservoir are about 510 and 185 m, respectively. The situations of the generated wave propagations in the near and far fields are shown in Fig. 12 for each scenario.

Wave amplitude The heights of the first generated wave for the first and the second scenarios are approximately 12 and 18 m, with

the positive wave amplitudes of 4.708 and 10.09 m and the negative wave amplitudes of 6.992 and 7.2 m, respectively. The time series of the first impulsive waves in the near field are shown in Fig. 13 for each scenario.

Wave run-up In the LS3D model, determination of wave run-up at the reservoir sidewalls follows the numerical approach of Synolakis who obtained a simple equation for estimating wave run-up (Eq. 12) from experiments on non-breaking positive solitary waves with non-permeable monotonously inclined sidewalls (Synolakis 1987).

$$\frac{R}{h_0} = 2.831 \left(\frac{H}{h_0} \right)^{1.25} \sqrt{\cot \beta} \quad (12)$$

where β is the slope angle of the run-up surface, R the run-up height, and H the height of the first wave close to the sidewall.

Wave run-up has been determined for each landslide scenario at several gauge locations near the sidewalls and the dam (Fig. 14). The run-up height at each gauge location, distance from landslide source

Table 4 The maximum wave amplitudes of each landslide scenario of the Shafa-Roud reservoir

Scenario no.	Max. positive wave amplitude (m)	Max. negative wave amplitude (m)	Maximum wave height (m)
1	8.1	18.5	27
2	9.8	21	31
3	9	21	30

Table 5 Wave run-up heights obtained by the LS3D and the FUNWAVE models, the Shafa-Roud dam

Gauge no.	Reservoir characteristics			Wave characteristics at gauges			Run-up height		
	Propagation distance x_p (m)	Average depth h_0 (m)	Beach slope β (deg)	Positive amplitude a_c (m)	Negative amplitude a_t (m)	Wave height H (m)	FUNWAVE R (m)	LS3D R (m)	Relative error Err (%)
11	750	90	20	(5.2) 5.3	(2.9)2.8	(8.1) 8.1	20.2	20.8	3.5
12	850	90	40	(4.5) 5.3	(2.2)2.4	(6.7)7.7	13.8	13	6.5
21	500	90	40	(5.2) 5.1	(3.3) 3.7	(8.5)8.9	18	15.3	15
22	600	90	45	(4.7)5.1	(2.7)3.3	(7.4)8.4	15	13.2	11.4
23	900	90	40	(3.3)5.7	(3.3)2.8	(6.6) 8.5	13.6	14.6	7.4
24	450	90	40	(6) 6.2	(3)4.9	(9)11.1	19.2	20.4	6.3
31	550	90	30	(6.2)6.8	(4.5) 3.1	(10.7)9.9	25.2	21.2	16

and the slope angle of sidewalls are listed in Table 2. The run-up height reaches approximately 30 m near the landslide source, revealing the fact that induced waves may cover extensive areas of the reservoir beaches.

Dam overtopping The levels of the Maku dam crest and the normal water are 1,690 and 1,680 m, respectively. A height of 1 m is estimated for the wind- and earthquake-generated waves. Thus, the dam freeboard is 9 m. In rainy seasons, the water level can rise close to the spillway level. The spillway of the Maku dam is a tunnel spillway in the left sidewall with a diagonal shaft, located at a level of 1,685 m. As it is more probable that landslides may initiate in rainy seasons, we consider the best (water level of 1,680 m) and the worst (water level of 1,685 m) conditions for estimating dam overtopping. The volume of overtopping water is calculated with the equation (Fritz et al. 2004):

$$V = b \int \eta dx = bc_c \int \eta dt \quad (13)$$

where V is the dam overtopping volume, b the dam crest length, η the positive wave amplitude over the dam crest level, c_c the wave crest propagation velocity and x and t the distance and the time interval during which the wave height close to the dam is higher than the dam crest level, respectively. The time series of water surface fluctuations is shown in Fig. 15 for each scenario.

The maximum wave heights close to the dam body are 7.8 and 8.5 m, with the positive wave amplitudes of 2.82 and 5.62 m and the wave crest propagation velocities of 16.4 and 18.8 m/s approximately, for each scenario, respectively. Thus, in the best condition, no overtopping happens. In the worst condition (the rainy seasons), the positive wave amplitude over the dam crest level is around 1.62 m for the second scenario and approximately 4,500 m³ of water is predicted to overtop the dam. Therefore, it seems that the 9 m freeboard of the Maku dam is enough to prevent overtopping a huge volume of water due to the considered landslide scenarios. In any case, a little amount of water always overtops the dam because of the generated wave run-up (Table 2).

Shafa-Roud dam reservoir

Setting

The Shafa-Roud dam site is located in the Western part of the Gilan province of Iran, 4 km away from the main city called Rezvan Shahr. The nearest downstream and upstream villages to the dam site are Poonel and Shalem, respectively, which are in danger due to the dam overtopping and subsequent flooding. Figure 16 shows the geographical situation of the dam site (Mahab Ghods 1999b).

The dam is located in a region highly susceptible to seismicity. The Astara fault is only a kilometer away from North of the dam. In

Table 6 The estimated dam overtopping volumes by the LS3D and the FUNWAVE models, Shafa-Roud dam

Scenario no.	Wave characteristics at gauges			Dam overtopping in the worst condition			Dam overtopping in the best condition		
	Positive amplitude a_c (m)	Negative amplitude a_t (m)	Wave crest propagation velocity c_c (m/s)	Positive wave amplitude higher than the dam-crest level H (m)	FUNWAVE V (m ³)	LS3D V (m ³)	Positive wave amplitude higher than the dam-crest level H (m)	FUNWAVE V (m ³)	LS3D V (m ³)
1	5.3	2.4	25.0	5.3	78,000	80,000	2.3	1,000	7,500
2	5.1	3.7	24.8	5.1	65,000	76,500	2.1	5,000	4,000
3	4.8	2.0	20.5	4.8	17,500	53,000	1.8	0	3,700

addition, the Hero-Abad, the Masooleh, and the North Alborz faults are only approximately 10, 40, and 70 km away from the dam site, respectively. The dam site is located in an approximately symmetrical narrow valley. On both sides of the valley, up to 215 m elevation, the slope is between 60% and 67%, decreasing in steepness towards higher elevation (Mahab Ghods 1999b).

The Shafa-Roud dam is a 150-m high gravity dam, with a reservoir capacity of 98 mm³. The reservoir length is about 7.5 km with an average width of 800 m. The total area of the reservoir in normal elevation is about 2.5 km². The dam crest length is roughly 500 m. To prevent overtopping, the dam freeboard of 3 m has been considered (Mahab Ghods 1999b).

Geological investigations have determined several likely slide regions near the dam axis and in the middle parts of the North side of the reservoir valley. These slide areas, consisted of sand stone and silt, are produced by the generated cracks, fractures, and faults caused by several factors such as increase in pore water pressure and human activities (Mahab Ghods 1999b). With the advent of slip signs in drilling boreholes in this area, the huge sliding potentials are supposed. In this paper, we focused on the three main landslide scenarios which will occur near the dam (Fig. 17).

The potential landslides are very close to the normal water level and the major part of them is located underwater. Ataie-Ashtiani and Malek-Mohammadi (2007) considered the slide as subaerial and used a minimum value for the slide impact velocity as 0.3 m/s based on the recommendation of Slingerland and Voight (1979). Then, they estimated the initial wave height and length by their empirical equations (Ataie-Ashtiani and Malek-Mohammadi 2008). In this work, it is considered that the potential landslides are submarine because their centers of gravity are under the water. In any case, they can be simulated by the extended numerical model, since they are partially submerged. The geometric characteristics of each scenario are summarized in Table 3.

Simulation set up

Time step and grid dimensions in x and y directions are chosen as 0.1 s and 20 m, respectively. The normal water level of the Shafa-Roud reservoir is 216 m and the reflection factor is estimated at 0.6.

Results

Wave amplitude The time series of the first generated waves for each landslide scenario of Shafa-Roud dam site are shown in Fig. 18. The properties of the waves are summarized in Table 4.

Wave run-up The wave run-up is estimated at the gauge locations shown in Fig. 17. The results are shown in Table 5. The three landslide scenarios of Shafa-Roud dam reservoir are also simulated by the FUNWAVE numerical model by (Ataie-Ashtiani and Malek-Mohammadi 2008). The results of each numerical approach are summarized in Table 5 and are observed to be in good agreement with relative error less than 15%.

Dam overtopping The levels of the Shafa-Roud dam crest and normal water are 220 and 216 m, respectively. This means the marginal height of 4 m is the sum of the dam's freeboard (3 m) and the height for the possible earthquake and wind generated waves (1 m). The Shafa-Roud dam has a free spillway at the level

of 220 m. Thus, the best (water level of 216 m) and the worst (water level of 220 m) conditions are considered to estimate the dam overtopping. The results for two numerical approaches are shown in Table 6 for each scenario considered.

Conclusions

A two-dimensional fully nonlinear higher-order Boussinesq-type model with moving bottom boundary, LS3D, has been used to study landslide-generated waves. The model has been newly extended for simulating impulsive waves caused by subaerial landslides entering a water body. A set of three-dimensional experimental data is used to validate the extended model. The numerical and the experimental results show good agreement. The time phase differences and the estimation error of the wave amplitudes are less than 15% and 5%, respectively. The estimation error of the wave amplitude for majority of the simulated experiments is less than 1%. Therefore, the extended model is able to simulate subaerial-landslide-generated waves with a degree of accuracy similar to that observed for the simulated submarine-landslide-generated waves in both generation and propagation stages.

The extended model is applied for simulating two real cases, the Maku and the Shafa-Roud dam reservoirs located in the northwestern and north of Iran. The generated wave heights, wave run-up, maximum wave height above the dam crest, and the dam overtopping volume have been evaluated for each case. For the Maku dam reservoir, two landslide scenarios have been simulated. Accordingly, a maximum positive near-field wave height of 18 m, maximum wave run-up of 30.7 m, and maximum downstream flood volume of 4,500 m³ have been estimated. Accordingly, the notable Maku dam freeboard of 9 m decreases the probability of overtopping an enormous volume of water and the following flooding in its downstream regions.

Finally, three landslide-generated wave scenarios at the Shafa-Roud dam site have been simulated. For this case, a maximum wave height of 31 m, maximum wave run-up of 21.2 m, and maximum dam flood volume of 80,000 m³ were estimated. Thus, it is possible that a vast downstream area is inundated with water, especially flat area such as residential, agricultural, or rural area. Besides, each coastal or hydraulic structure, especially those which are located near the sliding mass, can be threatened by generated wave's run-up. These results indicate the need for further examination of the impact of the impulsive waves induced by possible landslide events in the Maku and the Shafa-Roud dam reservoirs.

References

- Ataie-Ashtiani B, Malek-Mohammadi S (2007) Near field amplitude of sub-aerial landslide generated waves in dam reservoirs. *Dam Eng* XVII 4:197–222
- Ataie-Ashtiani B, Malek-Mohammadi S (2008) Mapping impulsive waves due to subaerial landslides into a dam reservoir: case study of Shafa-Roud dam. *Dam Eng* XVIII 3:1–25
- Ataie-Ashtiani B, Najafi-Jilani A (2006) Prediction of submerged landslide generated waves in dam reservoirs: an applied approach. *Dam Eng* XVII 3:135–155
- Ataie-Ashtiani B, Najafi-Jilani A (2007) A higher-order Boussinesq-type model with moving bottom boundary: applications to submarine landslide tsunami waves. *Intl J Numer Meth Fluid* 53(6):1019–1048
- Ataie-Ashtiani B, Nik-khah A (2008) Impulsive waves caused by subaerial landslides. *Environ Fluid Mech* 8(3):263–280

- Carvalho RF, Carmo JS (2007) Landslides into reservoirs and their impacts on banks. *Environ Fluid Mech* 7(6):481–493
- Enet F, Grilli ST, Watts P (2003) Laboratory experiments for tsunami generated by underwater landslides: Comparison with numerical modeling. *Proceeding of The 30th Intl Offshore and Polar Eng Conf, Hawaii, USA*, pp 372–379
- Enet F, Grilli S (2005) Tsunami landslide generation: modelling and experiments. *Ocean Wave Measurement and Analysis, Fifth Intl Symposium WAVES, Madrid, Spain*
- Fernandez-Nieto ED, Bouchut F, Bresch B, Castro Diaz MJ, Mangeney A (2008) A new Savage–Hutter type model for submarine avalanches and generated tsunami. *J Comput Phys* 227:7720–7754
- Fritz HM, Hager WH, Minor HE (2004) Near field characteristics of landslide generated impulse waves. *J Waterw Port Costal Ocean Eng* 130:287–302
- Gobbi MF, Kirby JT, Wei G (2000) A fully nonlinear Boussinesq model for surface waves. II. Extension to $O(kh^4)$. *J Fluid Mech* 405:181–210
- Grilli ST, Vogelmann S, Watts P (2002) Development of a 3D numerical wave tank for modeling tsunami generation by underwater landslides. *Eng Anal Bound Elem* 26:301–313
- Grilli ST, Watts P (1999) Modeling of waves generated by a moving submerged body; Applications to underwater landslides. *Eng Anal Bound Elem* 23:645–656
- Grilli ST, Watts F (2005) Tsunami generation by Submarine mass failure; I: modelling, experimental validation, and sensitivity analyses. *J of Waterway Port Costal and Ocean Eng, ASCE*, pp 283–297
- Hanes DM, Inman DL (1985) Experimental evaluation of a dynamic yield criterion for granular fluid flows. *J Geophys Res* 90(B5):3670–3674
- Heidarzadeh M, Pirooz MD, Zaker NH, Yalciner AC, Mokhtari M, Esmaily A (2008) Historical tsunami in the Makran subduction zone off the southern coasts of Iran and Pakistan and results of numerical modeling. *J Ocean Eng* 35:774–786
- Heinrich Ph, Piatanesi A, Hébert H (2001) Numerical modelling of tsunami generation and propagation from submarine slumps: the 1998 Papua New Guinea event. *J Int Geophys* 145:97–111
- Kirby JT, Wei G, Chen Q, Kennedy AB, Dalrymple RA (1998) FUNWAVE 1.0 fully nonlinear Boussinesq wave model documentation and user's manual. *Research Report No. CACR-98-06*
- Liu PLF, Wu TR, Raichlen F, Synolakis CE, Borrero JC (2005) Runup and rundown generated by three-dimensional sliding masses. *J Fluid Mech* 536:107–144
- Lynett P, Liu PL (2002) A numerical study of submarine-landslide-generated waves and run-up. *Phil Trans Roy Soc Lond UK A458:2885–2910*
- Lynett P, Liu PLF (2004) A multi-layer approach to wave modeling. *Proc Roy Soc Lond* 460:2637–2669
- Lynett P, Liu PLF (2005) A numerical study of the run-up generated by three-dimensional landslides. *J Geophys Res* 110:C03006. doi:10.1029/2004JC002443
- Mader CH (2002) Modeling the 1958 Lituya Bay mega-tsunami II. *Science of Tsunami Hazards* 20(5):241
- Mahab Ghods Inc (1999) Final report of the Maku dam reservoir project. (in Persian)
- Mahab Ghods Inc (1999) Final report of the Shafa-Roud dam reservoir project. (in Persian)
- Medina V, Hürlimann M, Bateman A (2008) Application of FLATMODEL, a 2D finite volume code, to debris flows in the northeastern part of the Iberian Peninsula. *Landslides* 5:127–142
- Najafi-Jilani A, Ataie-Ashtiani B (2007) Estimation of near-field characteristics of tsunami generation by submarine landslide. *Ocean Eng* 35:545–557
- Niro ministry (1999) Possible troubleshooting studies of the border rivers of Iran and Turkey; drainage network of Bazabgan plain. *Local water organization of west Azerbaijan province of Iran (in Persian)*
- Panizzo A, Girolamo PD, Di Risio M, Maistri A, Petaccia A (2005) Great landslide events in Italian artificial reservoirs. *Nat Hazards Earth Syst Sci* 5:733–740
- Pastor M, Herreros I, Fernández Merodo JA, Mira P, Haddad B, Quecedo M, González E, Alvarez-Cedrón C, Drempevic V (2008) Modelling of fast catastrophic landslides and impulse waves induced by them in fjords, lakes and reservoirs. *J Eng Geol* 29:124–134
- Risio M, Bellotti G, Panizzo A, Girolamo PD (2009) Three-dimensional experiments on landslide generated waves at a sloping coast. *Coast Eng* 56:659–671
- Saut O (2003) Determination of dynamic stability characteristics of an underwater vehicle including free surface effects. *MS Thesis, Florida Atlantic University, No of pages 149*
- Semenza E (2000) La storia del Vajont, raccontata dal geologo che ha scoperto la frana. *Tecomproject, Ferrara*
- Shigihara Y, Goto D, Imamura F, Kitamura Y, Matsubara T, Takaoka K, Ban K (2006) Hydraulic and numerical study on the generation of a subaqueous landslide-induced tsunami along the coast. *Nat Hazards* 39:159–177
- Slingerland RL, Voight B (1979) Occurrences, properties, and predictive models of landslide-generated water waves. In: *Developments in Geotechnical Engineering 14B: Rockslides and Avalanches, 2, Engineering Sites*. Voight B, ed., Elsevier Scientific Publishing Company, pp 317–397
- Synolakis CE (1987) The run-up of solitary waves. *J Fluid Mech* 185:523–545
- Zweifel A, Hager WH, Minor HE (2006) Plane impulsive waves in reservoirs. *Journal of Waterway, Port, Costal, and Ocean Engineering* 132:358–368. doi:10.1061/(ASCE)0733-950X

B. Ataie-Ashtiani (✉) · **S. Yavari-Ramshe**

Department of Civil Engineering,
Sharif University of Technology,
Tehran, Iran
e-mail: ataie@sharif.edu

S. Yavari-Ramshe
yavari@mehr.sharif.edu